Contrib Mineral Petrol (2004) 148: 131–149
DOI 10.1007/s00410-004-0598-7

ORIGINAL PAPER

Wilhelm Heinrich · Sergey S. Churakov
Matthias Gottschalk

Mineral-fluid equilibria in the system $CaO–MgO–SiO_2–H_2O–CO_2–NaCl$ and the record of reactive fluid flow in contact metamorphic aureoles

Received: 21 January 2004 / Accepted: 10 June 2004 / Published online: 5 August 2004

Abstract Phase equilibria in the system $CaO–MgO–SiO_2–CO_2–H_2O–NaCl$ are calculated to illustrate phase relations in metacarbonates over a wide-range of P–T–X[$H_2O–CO_2–NaCl$] conditions. Calculations are performed using the equation of state of Duan et al. (Geochim Cosmochim Acta 59:2869–2882, 1995) for $H_2O–CO_2–NaCl$ fluids and the internally consistent data set of Gottschalk (Eur J Mineral 9:175–223, 1997) for thermodynamic properties of solids. Results are presented in isothermal-isobarical plots showing stable mineral assemblages as a function of fluid composition. It is shown that in contact-metamorphic P–T regimes the presence of very small concentrations of NaCl in the fluid causes almost all decarbonation reactions to proceed within the two fluid solvus of the $H_2O–CO_2–NaCl$ system.

Substantial flow of magma-derived fluids into marbles has been documented for many contact aureoles by shifts in stable isotope geochemistry of the host rocks and by the progress of volatile-producing mineral reactions controlled by fluid compositions. Time-integrated fluid fluxes have been estimated by combining fluid advection/dispersion models with the spatial arrangement of mineral reactions and isotopic resetting. All existing models assume that minerals react in the presence of a single phase $H_2O–CO_2$ fluid and do not allow for the effect that fluid immiscibility has on the flow patterns.

It is shown that fluids emanating from calc-alkaline melts that crystallize at shallow depths are brines. Their salinity may vary depending mainly on pressure and fraction of crystallized melt. Infiltration-driven decarbonation reactions in the host rocks inevitably proceed at the boundaries of the two fluid solvus where the produced CO_2 is immiscible and may separate from the brine as a low salinity, low density $H_2O–CO_2$ fluid. Most parameters of fluid–rock interaction in contact aureoles that are derived from progress of mineral reactions and stable isotope resetting are probably incorrect because fluid phase separation is disregarded.

Editorial Responsibility: J. Hoefs

W. Heinrich (✉) · S. S. Churakov · M. Gottschalk
GeoForschungsZentrum Potsdam, Division 4,
Telegrafenberg, 14773 Potsdam, Germany
E-mail: whsati@gfz-potsdam.de
Tel.: +49-331-2881410
Fax: +49-331-2881402

Introduction

Many fluid inclusion studies in contact and regional metamorphic calcareous rocks have revealed that $H_2O–CO_2$ immiscibility occurred in the presence of dissolved salts (Sisson et al. 1981; Mercolli 1982; Trommsdorff et al. 1985; Williams-Jones and Ferreira 1989; Heinrich 1993; Jamtveit and Andersen 1993; Heinrich and Gottschalk 1994, 1995; Fernandez-Caliani et al. 1996). Based on the experimental work of Gehrig (1980), Bowers and Helgeson (1983a, b) developed a modified Redlich–Kwong (MRK) equation of state (EOS) for $H_2O–CO_2–NaCl$ fluids that allowed for equilibrium calculations of mineral reactions in metamorphic rocks in this fluid ternary. With that, Trommsdorff and Skippen (1986) and Skippen and Trommsdorff (1986) have derived fluid evolution paths for $H_2O–CO_2–NaCl$ fluids during reaction progress in metamorphosed impure limestones. They showed that the development of prograde mineral reactions is intensely affected if CO_2-loss by boiling occurs.

A major shortcoming of the MRK–EOS of Bowers and Helgeson (1983a) is that it is unable to accurately predict fugacities of fluid components near the solvus boundaries and at moderate and high salinites. Therefore, phase diagrams presented by Trommsdorff and Skippen (1986) that combine dehydration/decarbonation reactions with thermodynamic properties of immiscible fluids in the $H_2O–CO_2–NaCl$ ternary are semi-quantitative. An EOS more convenient for rigorous thermodynamic modelling of $H_2O–CO_2–NaCl$ flu-

ids was introduced by Duan et al. (1995). It can be applied to a temperature range of 300–1,000°C, pressures up to 600 MPa, and calculates activities of fluid components for compositions of up to 30 wt% NaCl (relative to H_2O–NaCl) in good agreement with experimental results, and for fluids of up to 50% NaCl with somewhat less accuracy. Furthermore, it predicts halite solubility in CO_2-poor brines within the error of the experimental data and with less precision in NaCl-poor H_2O–CO_2 fluids. In the first part of this study, quantitative phase relations in the system CaO–MgO–SiO_2–CO_2–H_2O–NaCl are calculated by combining the EOS of Duan et al. (1995) with thermodynamic properties of solids from the internally consistent data set of Gottschalk (1997) using Gibbs free energy minimization methods. Following Trommsdorff and Skippen's (1986) delineation, phase relations and mineral reactions are presented in a series of isobarical-isothermal sections through the H_2O–CO_2–NaCl ternary in the T-range from 350 to 900°C in steps of 50°C at various pressures. We will show that, under the low pressure regime of contact metamorphism, very small amounts of NaCl in the fluid systems are sufficient for most decarbonation reactions to proceed within the two fluids immiscibility field of the H_2O–CO_2–NaCl system.

It has been shown for many contact aureoles that fluid infiltration controls the mineralogical and stable isotope composition of rocks during metamorphism (e.g. Heinrich 1993; Ferry 1995, 1996; Heinrich and Gottschalk 1995; Ferry and Rumble 1997; Holness 1997; Holness and Fallick 1997; Povoden et al. 2002). This is particularly true for contact metamorphic metacarbonates where significant shifts in oxygen isotope ratios indicate substantial flow of magma-derived fluids into the host rocks. The progress of volatile-producing mineral reactions has been interpreted in terms of time-integrated fluid fluxes by combining fluid advection/dispersion models with the spatial arrangement of mineral reactions and isotopic resetting (e.g. Labotka et al. 1988; Nabelek et al. 1992; Jamtveit et al. 1992a, b; Bowman et al. 1994; Gerdes et al. 1995; Dipple and Ferry 1996; Cartwright and Buick 1996; Cartwright 1997; Cook et al. 1997; Ferry et al. 1998). Summarizing field data of many contact aureoles, Ferry and Gerdes (1998), Baumgartner and Valley (2001) and Ferry et al. (2002) offered global reviews on stable isotope transport and direction of contact metamorphic fluid flow in metacarbonate host rocks worldwide.

However, all presented models generally assume that the magma-derived infiltrating fluid is pure water and that decarbonation/dehydration reactions occurred in the presence of a single phase H_2O–CO_2 fluid. Adapting arguments of Cline and Bodnar (1991), Webster (1997) and Webster et al. (1999), we show in the second part of the study that fluids expelled by magmas at shallow intrusion levels are brines. It is most likely that all contact-metamorphic decarbonation reactions triggered by them occur within the two fluid solvus. This is, with very few exceptions, not recognized. Since existing models do not allow for the effect that fluid immiscibility has on flow patterns, fluid flow in contact-metamorphic carbonates is probably not adequately described and, in principle, not understood. We argue that existing field data of mineral reaction distributions and oxygen alterations in contact aureoles should be reinterpreted in terms of fluid immiscibility and speculate on inconsistencies between field data and existing models, which arise because fluid separation is ignored.

Phase relations in the system H_2O–CO_2–NaCl

Semi-quantitative phase relations in the system H_2O–CO_2–NaCl have been presented by Trommsdorff and Skippen (1986) and Skippen and Trommsdorff (1986), using a series of isothermal-isobaric sections through the ternary system at various P–T conditions. The main features of the phase topology, now calculated with the EOS of Duan et al. (1995), are shown in Fig. 1. Six isothermal-isobaric sections of the ternary are placed onto a P–T projection ranging up to 1,000°C and 600 MPa, along with phase relations of the respective binaries H_2O–CO_2, H_2O–NaCl, CO_2–NaCl, and the melting curve of halite. The essential points are summarised as follows:

1. The critical curve of the H_2O–CO_2 binary, indicated as L + V = supercritical fluid (SCF), lies always below 350°C except at conditions close to the critical point of pure water (T_c). At $T > T_c$, a binary H_2O–CO_2 mixture is always homogeneous within the given pressure range.
2. The topology of the CO_2–NaCl binary is controlled by the melting curve of halite (Hl) at high T (Hl = L). The critical curve is not well known but it is clear that $NaCl^{liquid}$ and CO_2 are extremely immiscible, even at very high temperatures. Fluids of the CO_2–NaCl binary are likely two-phase for any geological process in the crust. At T below the melting curve of halite, a field of halite-liquid equilibrium occupies the NaCl-rich part of the CO_2–NaCl binary (II and V in Fig. 1). Below 800°C, halite coexists with almost pure CO_2 because of the very low solubility of halite in CO_2 vapour (I and IV).
3. In the H_2O–NaCl binary, halite coexists with a single-phase brine at pressures above the critical curve (indicated as L + V = SCF). At lower pressure, a V + L field appears (IV in Fig. 1). At very low pressures, a V + Hl field exists which is bound by the V + Hl = L curve. Above the halite melting curve, at high pressure a single brine exists (III), and at low pressure NaCl-rich brine coexists with NaCl-poor vapour (VI).
4. In the H_2O–CO_2–NaCl ternary, phase relations of type I and IV are characteristic for the major part of the P–T space. The peculiar property of these topol-

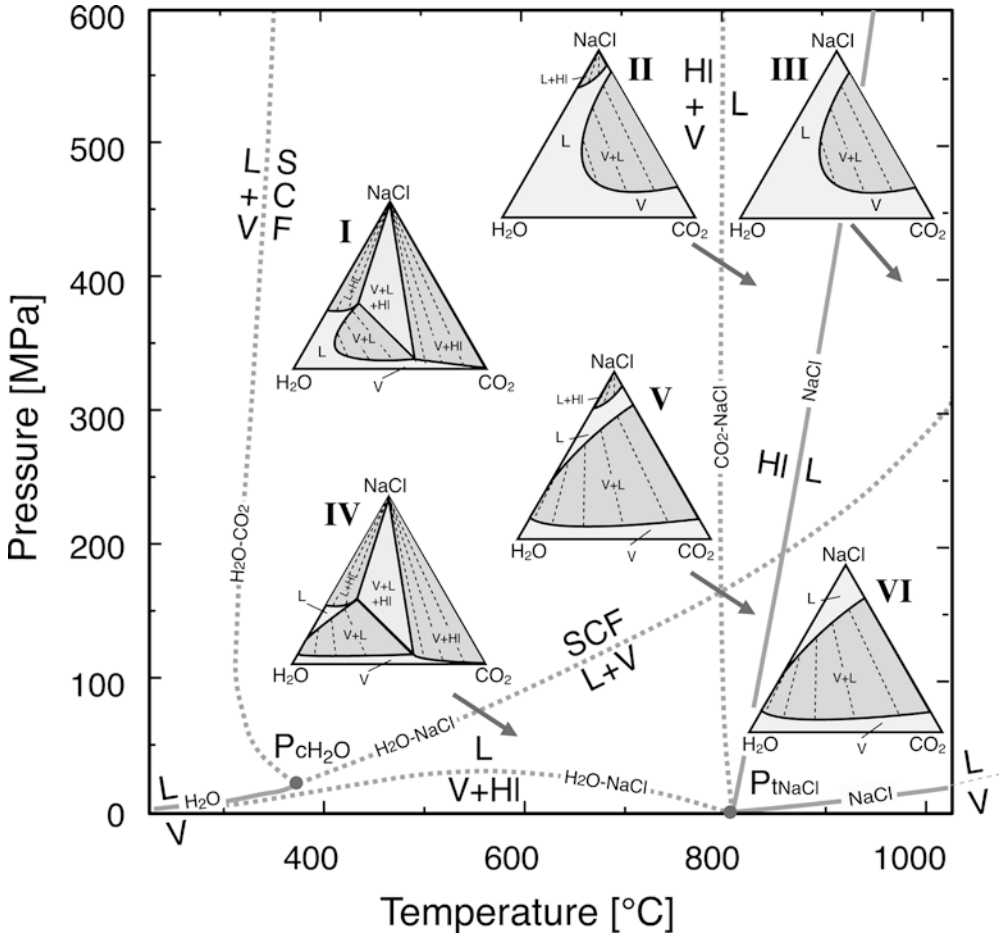

Fig. 1 Pressure–temperature plot of the H_2O–CO_2–NaCl ternary, modified after Trommsdorff and Skippen (1986). Components are given in mol%. Binary curves and isothermal-isobarical sections through the ternary are calculated with the EOS of Duan et al. (1995). Data for halite and $NaCl^{liquid}$ are from the Glushko (1976–1982) database. *Thin broken lines* within the two-phase fields indicate calculated compositions of coexisting liquid and vapour

ogies is that large fields of V + L and V + L + HL equilibria occur. In the water-rich part, NaCl-rich, CO_2-poor brine coexists with NaCl-poor vapour, which is richer in CO_2. The V + L + HL field shrinks with increasing temperature in favour of the V + L field because of increasing solubility of NaCl in the brine.

5. The extension of the V + L field is strongly dependent on pressure, particularly near the H_2O apex. It is widely open at low pressure (IV and V) and shrinks in favour of the one phase field as pressure increases (I, II, and III).
6. Our calculated V – L tie lines in isothermal-isobaric sections I and IV are significantly steeper than those estimated by Trommsdorff and Skippen (1986). This is because a large V + HL field exists at low and medium T, where the X_{CO_2} of vapour coexisting with halite-saturated brine cannot exceed 0.6 at most conditions.
7. At most metamorphic conditions, a three component H_2O–CO_2–NaCl system consists of at least two phases. This is particularly true for low-pressure contact-metamorphism where very small amounts of NaCl are sufficient to create a solvus between brine and H_2O–CO_2-bearing vapour, which is nearly NaCl-free.

Phase relations in the system CaO–MgO–SiO_2–H_2O–CO_2–NaCl

Phase relations in the system CaO–MgO–SiO_2–H_2O–CO_2–NaCl have been calculated for three different bulk compositions A, B, and C in the CMS subsystem (Fig. 2). A is quartz-rich and stands for calc-silicate marble, B and C are dolomite-rich representing dolomite-calcite marbles with different quartz/carbonate-ratios. Twenty-four solid phases were taken into account (Fig. 2). Thermodynamic properties of minerals, H_2O and CO_2 are from Gottschalk's (1997) internally consistent data set, that of halite and halite melt from the Glushko (1976–1982) database (Table 1). Fugacities of fluid components in the H_2O–CO_2–NaCl ternary are calculated using the EOS of Duan et al. (1995). Calculations are based on a Gibbs free energy minimization program available upon request from one of the authors. Computation allows input of pure phases and/or non-ideal solid solutions. Some calculations were performed using properties for pure calcite and dolomite as well as for pressure–temperature dependent calcite–dolomite solid solutions (Gottschalk and Metz 1992). Comparison of the results shows very small differences for the P–T dependence of mineral stabilities, which lie

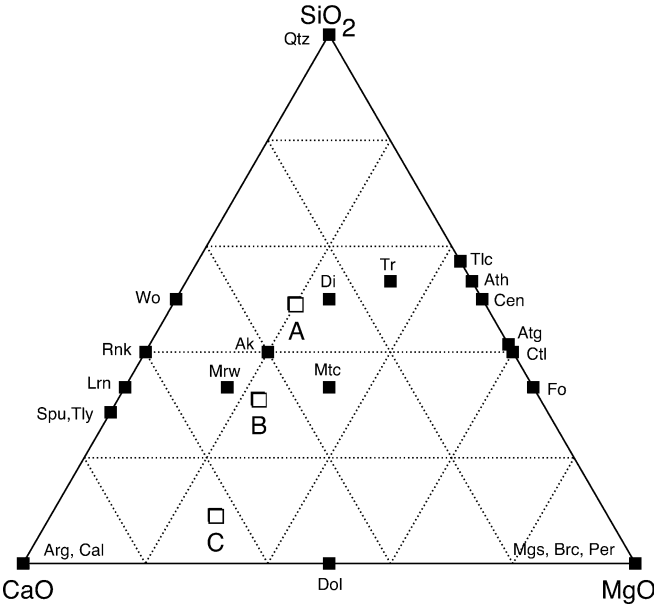

Fig. 2 Composition triangle for the system CaO–MgO–SiO_2–H_2O–CO_2–NaCl projected from H_2O, CO_2 and NaCl showing positions of minerals considered for stability calculations. Formulae and abbreviations as in Table 1. *A*, *B*, and *C* denote the three different bulk compositions used in calculations of stable phase assemblages by Gibbs free energy minimization methods

within the accuracy range for fugacities of fluid components given by the EOS of Duan et al. (1995). To keep computation simple and fast, properties of pure calcite and dolomite were used.

The results are illustrated using a series of isobaric-isothermal sections of the system H_2O–CO_2–NaCl indicating the stability regions of isothermal-isobarically divariant three solid assemblages (Fig. 3). In the one fluid field these are separated by univariant reaction curves (black lines in Fig. 3). Reaction curves are isothermal-isobarically invariant (dotted lines) where a second fluid phase or halite additionally appears. Isothermal-isobaric invariant points in the one fluid field, where two reactions intersect, do not become visible in these sections because they lie outside the applied plotting range in steps of 50°C, but are present in between at distinct P–T–X conditions. A detailed discussion of the stability fields of mineral assemblages and respective reaction curves relative to the fluid solvus in P–T–X space is presented elsewhere, and the consequences for metamorphic reaction progress is illustrated by means of two important decarbonation reactions below. Here, we briefly consider some general features, particularly the differences between contact and regional metamorphic conditions.

Figure 3a shows mineral assemblages of siliceous limestone A in the presence of NaCl from 350 to 900°C in steps of 50°C for 50 and 200 MPa, respectively. For both pressures, the well-known sequence of the prograde index minerals talc, tremolite, diopside, wollastonite, monticellite, and akermanite develops with increasing temperature. Because they are formed by decarbonation reactions, including hydration and dehydration for reactions involving talc and tremolite, they first appear at the water-rich side of the ternary diagrams. As temperature increases, reaction curves are generally shifted towards the CO_2 apex eventually intersecting the two fluid solvus and, in some cases, arriving again in a one fluid field where the fluid phase is CO_2-rich, almost NaCl-free, and coexists with halite. This behaviour is seen, for example, in sections at 450 and 500°C, 200 MPa (Fig. 3a). At 450°C, two assemblages appear, Qtz + Cal + Dol and Qtz + Tr + Cal, which are separated by the reaction Dol + Qtz + $H_2O \Leftrightarrow$ Tr + Cal + CO_2 (black line). This reaction curve lies in the one fluid field, very close to the solvus boundary. A few degrees above, the reaction shifts into the solvus, where two immiscible fluids are produced. At 500°C, the reaction curve has already moved into the vapour + halite field (dotted line) where a single CO_2-rich, NaCl-free fluid along with halite is present. At the water-rich side, two new assemblages appear in the one-fluid field, Qtz + Di + Cal and Wo + Di + Cal, due to the reactions Cal + Qtz + Tr $\Leftrightarrow$ Di + CO_2 + H_2O, and Cal + Qtz $\Leftrightarrow$ Wo + CO_2, respectively, the latter evolving in a comparable way from 500°C up to 700°C (Fig. 3a, right column). Similarly, the evolution of mineral assemblages for bulk compositions B and C is shown in Fig. 3b, c. For composition B, the sequence with increasing temperature at the water-rich side of the ternary is talc, tremolite, antigorite, diopside, forsterite, monticellite, akermanite, tilleyite, spurrite, merwinite, and periclase. For composition C it is talc, tremolite, antigorite, forsterite, brucite, periclase, monticellite and merwinite. Figure 3d shows isothermal-isobaric sections for bulk compositions A and C at ten P–T conditions that represent a schematic regional metamorphic P–T path. Prograde metamorphism with increasing pressure and temperature is traced from 50 MPa, 350°C to 500 MPa, 500°C (five sections from below), followed by increasing temperature from 550 to 650°C at 500 MPa (next three sections) and two sections showing retrograde conditions at 300 MPa, 550°C and 100 MPa, 400°C (above).

The diagrams highlight the relative positions of mineral assemblages and reaction curves with respect to the two-fluid solvus, the two fluid + halite, and the vapour + halite stability field. At 50 MPa and above 450°C, minute amounts of NaCl in the fluid system lead most reactions into the two fluid solvus or in the vapour + halite field. As pressure increases at identical temperatures (see respective diagrams at 200 MPa), mineral stability fields and reaction curves shift towards the H_2O apex, whereas the solvus shrinks in the opposite direction. It is obvious that the position of a particular reaction relative to the two fluid solvus may be very sensitive to small pressure and temperature variations. Most reactions along the prograde stages of a typical regional metamorphic P–T path occur within the water-

Table 1 Thermodynamic properties of phases in the system CaO–MgO–SiO_2–H_2O–CO_2–NaCl. Data are from Gottschalk (1997), for halite and supercooled halite melt from the Glushko database (1976–1982)

Phase	Abbreviations	Composition	$\Delta_f H°$ (kJ/mol)	$S°$ (J/(K mol))	T (K)	Cp (J/(K mol))						$V°$ (cm^3/mol)	a ($\times 10^5$)	b ($\times 10^6$)
						a	b ($\times 10^3$)	c ($\times 10^5$)	d ($\times 10^{-2}$)	f ($\times 10^{-5}$)	g ($\times 10^{-7}$)			
Akermanite	Ak	$Ca_2MgSi_2O_7$	−3863.679	212.413	298	445.11	−51.463	2.186	−37.937			92.81	3.00	14.0
					1,100	389.64			−29.656		−18.333	92.81	3.00	14.0
Anthophyllite	Ath	$Mg_7Si_8O_{24}H_2$	−12069.03	534.521	298	1259.9	18.884		−81.274	−116.427		264.47	3.00	12.0
Antigorite	Atg	$Mg_{48}Si_{34}O_{147}H_{62}$	−71444.33	3596.317	298	9,012			−639.81	−1459.62	1907.02	1749.13	3.20	20.6
Aragonite	Arg	$CaCO_3$	−1205.554	91.341	298	81.53	45.673			−11.405		34.15	7.27	15.5
					600	166.62			−14.994		5.449	34.15	7.27	15.5
Brucite	Brc	$Mg(OH)_2$	−925.247	63.141	298	102.22	15.107			−26.172		24.63	3.25	25.0
					500	136.84			−5.371	−43.619	55.269	24.63	3.25	25.0
Calcite	Cal	$CaCO_3$	−1206.686	91.487	298	99.72	26.92			−21.576		36.93	2.85	13.7
					650	193.24			−20.409		19.946	36.93	2.85	13.7
Chrysotile	Ctl	$Mg_6Si_4O_{18}H_8$	−8723.187	442.159	298	1079.5			−61.446	−289.252	394.752	214.44	3.32	20.8
Clinoenstatite	Cen	$Mg_2Si_2O_6$	−3091.616	135.779	298	411.12	−25.592		−45.954	23.852		62.56	2.87	7.3
Diopside	Di	$CaMgSi_2O_6$	−3200.639	142.842	298	191.82	83.079	−2.172		−42.795		66.09	3.34	8.47
Dolomite	Dol	$CaMgC_2O_6$	−2325.463	155.411	298	547.88	−167.59	7.708	−65.479	28.4		64.34	3.74	12.2
					900	368.02			−37.508		18.079	64.34	3.74	12.2
Forsterite	Fo	Mg_2SiO_4	−2174.663	94.283	298	87.36	87.17	−2.237	8.436	−36.99		43.79	3.81	7.30
Halite	Hl	NaCl	−411.26	72.12	298	45.151	17.947					27.005	15.00	4.0
Larnite	Lrn	Ca_2SiO_4	−2304.837	127.306	298	249.69			−20.943			51.6	3.80	9.45
					970	161.62		1.89				59.11	3.80	9.45
Magnesite	Mgs	$MgCO_3$	−1111.973	65.084	298	81.12	52.254			−18.32		28.02	3.73	8.20
					800	194.08			−21.21	−1.533	17.491	28.02	3.73	8.20
Merwinite	Mrw	$Ca_3MgSi_2O_8$	−4545.221	253.267	298	453.62			−32.5		−34.423	104.4	4.00	11.1
Monticellite	Mtc	$CaMgSiO_4$	−2251.617	108.133	298	231.4	−0.853	−0.133	−16.234	−12.474		51.47	3.75	8.15
Periclase	Per	MgO	−601.349	26.95	298	65.21	−1.27		−3.872	−4.619		11.25	3.95	5.9
Quartz α	Qtz	SiO_2	−910.7	41.46	298	81.14	18.283	0.541	−6.985	−1.81		22.69	4.40	25.0
Quartz β	Qtz				844	57.96	9.33			18.347		23.414	0.00	25.0
Rankinite	Rnk	$Ca_3Si_2O_7$	−3941.902	210.137	298	473.21	−42.071		−43.188	3.397		96.51	2.50	14.2
Spurrite	Spu	$Ca_5Si_2O_{11}C_1$	−5855.558	325.873	298	99.72	453.264	−16.3	33.128	−68.777		148.03	2.50	11.2
Talc	Tlc	$Mg_3Si_4O_{12}H_2$	−5894.911	260.04	298	664.11			−51.872	−21.472	32.737	136.25	2.86	20.0
Tilleyite	Tly	$Ca_5Si_2O_{13}C_2$	−6362.5	390.877	298	672.64	11.769		−43.188	−39.755		172.03	2.50	15.6
Tremolite	Tr	$Ca_2Mg_5Si_8O_{24}H_2$	−12306.93	549.209	298	2102.7	−471.69	11.146	−241.46	76.31		272.92	3.00	15.0
Wollastonite	Wo	$Ca_2Si_2O_6$	−3265.298	163.532	298	289.07			−10.91	−87.878	120.178	79.86	2.43	15.0
					995	270.06			−6.396			79.86	2.43	15.0
Water		H_2O	−241.814	188.72	298	10.438	25.955		2.992	−1.311				
CO_2		CO_2	−393.51	213.79	298	87.82	−2.6442		−998.86	7.064				
$Halite_{melt}$		NaCl	−390.666	83.425	298	67.9								

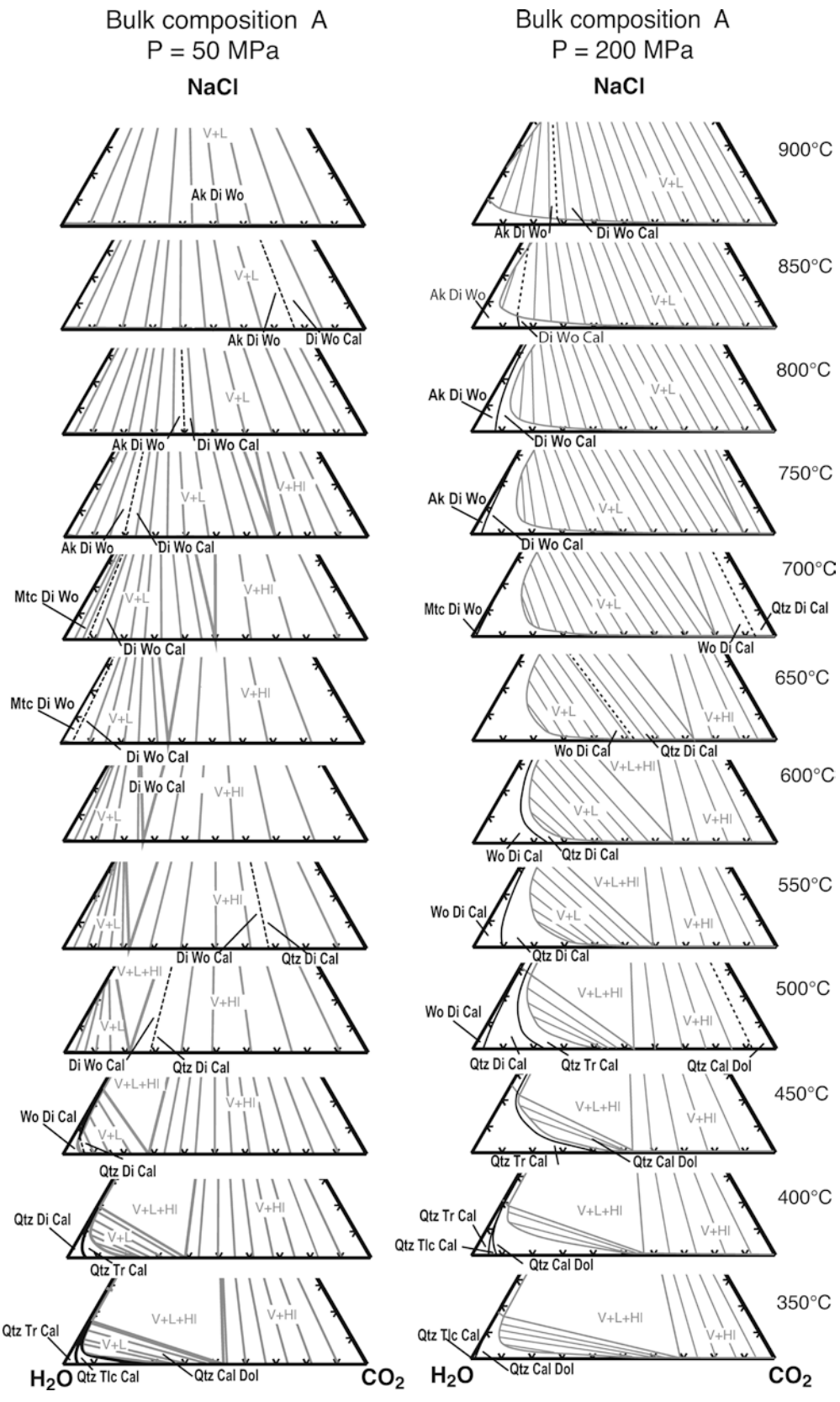

Fig. 3a–d Isobaric isothermal sections of the system H_2O–CO_2–NaCl showing the stability regions for mineral assemblages in siliceous dolomites and limestones at various temperatures at 50 and 200 MPa for bulk compositions A (**a**), B (**b**) and C (**c**), and at various P–T for bulk compositions A and C (**d**). Data and abbreviations are from Table 1. *Grey* fluid phase relations. In the one fluid phase field, isobaric isothermal divariant three solid assemblages are separated by univariant reaction curves (*solid black lines*); within the solvus the two reaction points (*connected by dotted tie lines*) are isothermal-isobarically invariant. A degenerated Tlc + Cal two-phase field (**b**, *below*) exists because bulk composition B lies on the Tlc–Cal tie-line. Invariant points in the one fluid field, where two reactions intersect, do not appear in these sections but are present at distinct P–T–X conditions

rich part of the one fluid field, irrespective of salinity. Thus, fluid immiscibility probably plays a minor role during regional metamorphism. At the low pressure, high temperature regime of contact metamorphism, however, fluid immiscibility has a tremendous effect on the reaction history of metacarbonates.

Fig. 3a–d (Contd.)

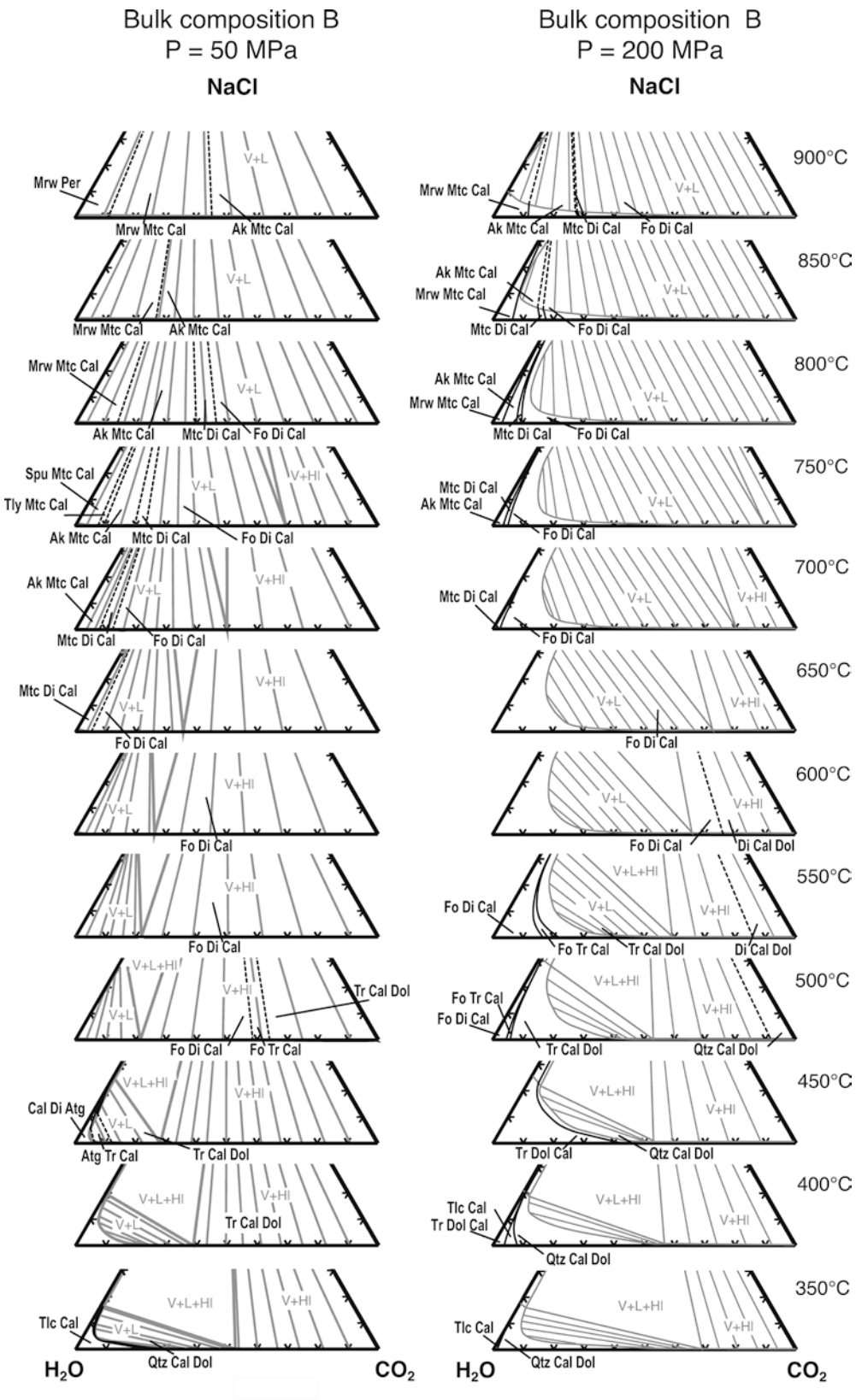

Fig. 3a–d (Contd.)

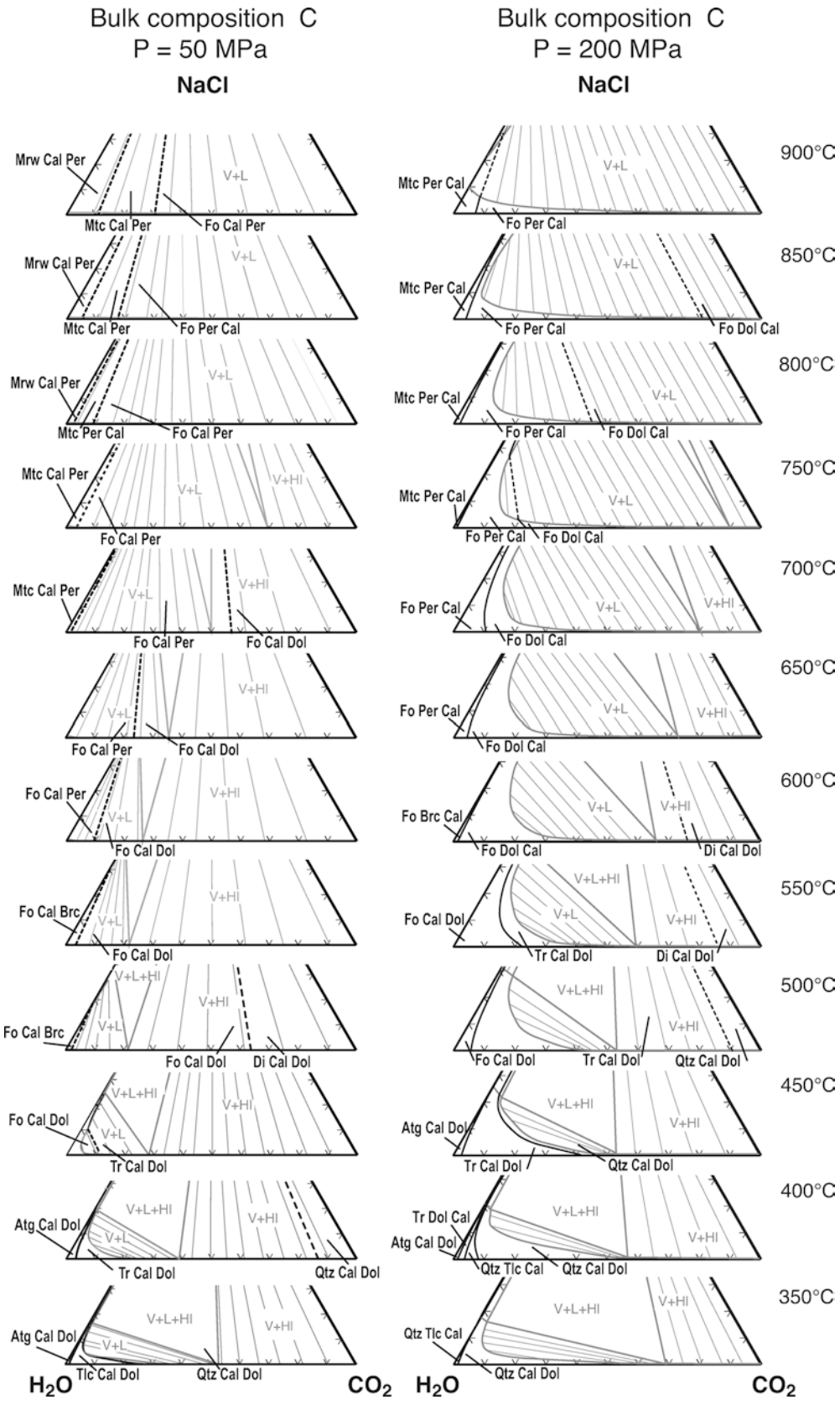

Fig. 3a–d (Contd.)

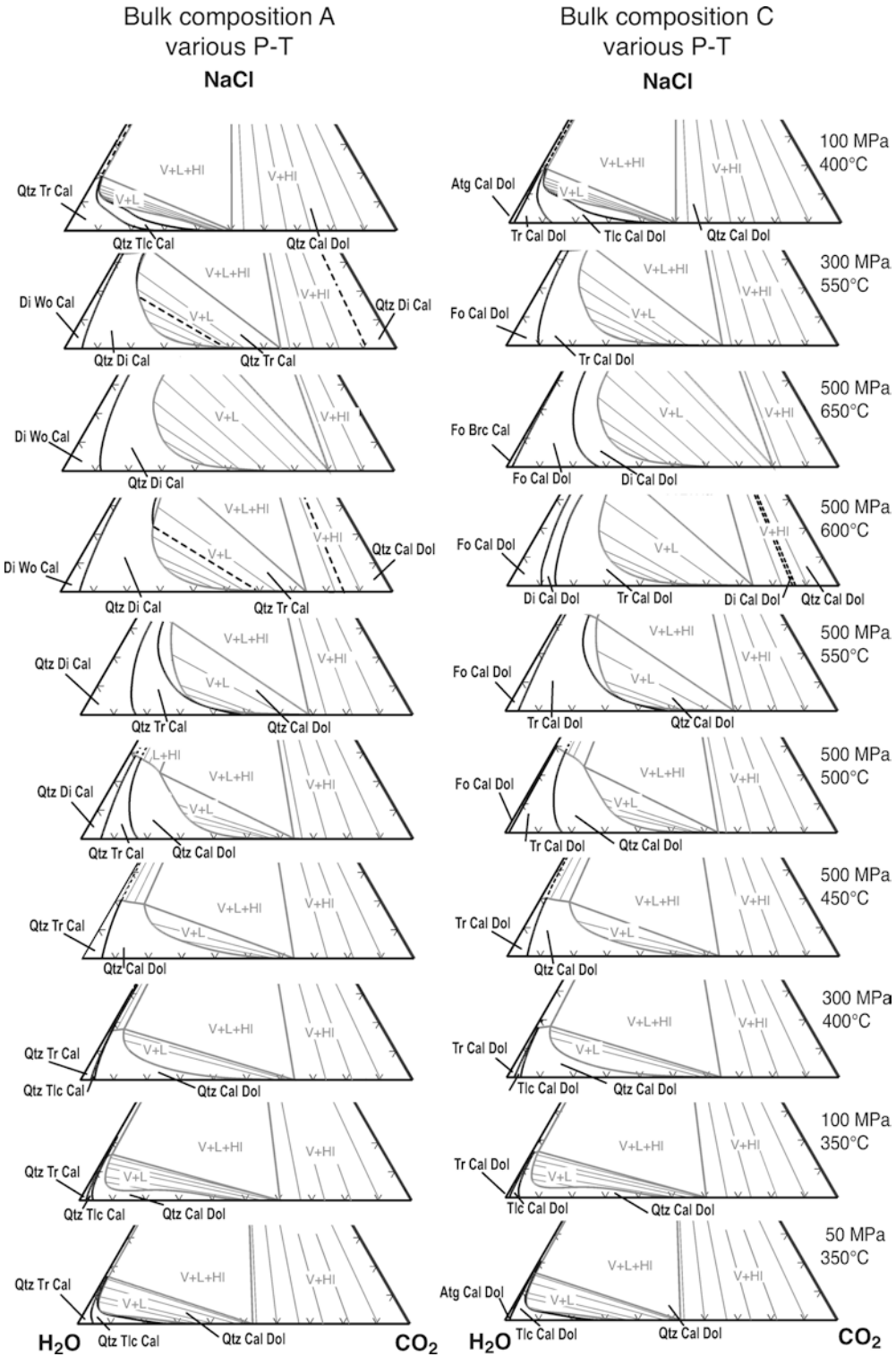

Salinity of fluids exsolved by aluminosilicate melts at shallow levels

The most important volatiles in magmas are water and chlorine. Though chlorine is generally far less abundant than water in melts, it exerts a strong influence on late magmatic and hydrothermal processes. Magmatic crystallization increases volatile abundances in residual melts, finally driving them towards volatile phase saturation. This induces second boiling, that is crystallization-induced exsolution-degassing resulting from increasing volatile fugacities within residual fractions of silicate melt. The crystallization of water- and chloride-free phases enriches the residual fractions of silicate melt

until the volatile solubility limits are exceeded and vapour, liquid, or supercritical fluid exsolve. If infiltrating into country rocks, the progress of volatile-producing mineral reactions and the shifts in stable isotope geochemistry is controlled by the compositions of these fluids.

The role of chlorine in magmatic degassing has been addressed by a large number of studies including experimental work (e.g. Shinohara et al. 1989; Shinohara 1994; Williams et al. 1995; Webster 1997; Webster et al. 1999; Webster and DeVivo 2002), melt and fluid inclusion studies (e.g. Lowenstern 1994, 1995; Webster et al. 1999; Webster and Rebbert 2001; Webster 2002) and numerical modelling (e.g. Cline and Bodnar 1991; and references above). These and many other studies show that exsolution of magmatic volatile phases is a complex process controlled mainly by pressure, temperature, and composition of aluminosilicate melts, which in turn dictate their water and chlorine solubility limits. The composition of exsolved fluids is a function of the partitioning behaviour of components between silicate melt and fluid, and compositions change with time as distillation proceeds. A detailed review is beyond the scope of this paper and we briefly concentrate on aspects concerning the evolution of magmatic volatile phases and the fate of chlorine during degassing.

Data from the literature on chlorine contents of pre-eruptive silicate melt inclusions from a variety of igneous rocks have been collected by Webster (1997, 2002) and Webster et al. (1999). The vast majority of rhyolitic, dacitic and andesitic melts have chlorine contents ranging between 0.1 and 0.45 wt% with an average at about 0.25 wt%. Chlorine contents in basaltic melt inclusions ranges from 0.05 to 0.75 wt%, and strongly alkaline melt inclusions have between 0.9 and 1.2 wt% Cl. Compositions of coexisting fluid inclusions from numerous igneous systems imply that these melts exsolved brines (sometimes also termed hydrosaline liquids or hydrous chloride melts). Brine may form by subcritical phase separation of exsolved fluid to vapour and brine, or may exsolve directly from magma (e.g. Webster 2002). The likelihood that a single alkali chloride bearing volatile phase unmixes to form vapour and hydrous chloride melt increases with decreasing pressure or increasing temperature (Webster and DeVivo 2002). This is immediately seen using a P–T–X_{NaCl}-plot, which roughly approximates compositions of coexisting vapour and brine in complex natural systems (Fig. 4; data from Bodnar et al. 1985).

The degassing process of a typical calc-alkaline melt has been modelled by Cline and Bodnar (1991) using experimentally determined fluid-melt partition coefficients for water and chlorine of Shinohara et al. (1984, 1989), taking also into account biotite crystallization that removes a small amount of water during crystallization. The model melt has 2.5 wt% water and a Cl/H_2O-ratio of 0.1 at 700°C. At 200 MPa and upon 60% of crystallization, the melt attains water saturation at 6 wt% H_2O, and a single phase brine exsolves that has a

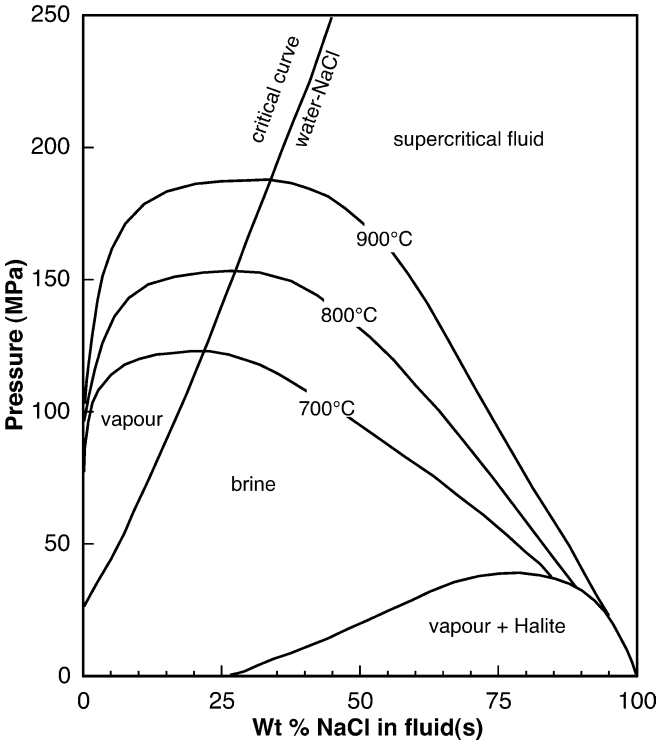

Fig. 4 Plot of NaCl concentration vs. pressure for coexisting brine plus vapour at magmatic conditions of 700, 800, and 900°C. Solvi shrink with increasing pressure and expand with increasing temperature. Data from Bodnar et al. (1985)

salinity of about 53 wt% NaCl (Fig. 5). This is because chlorine at 200 MPa partitions strongly into fluid and because it occurs beyond the brine-vapour immiscibility field (Fig. 4). The remaining melt is strongly depleted in chlorine and successively exsolved aliquots contain lower chlorine concentrations. Webster and Rebbert (1999) observed this trend in a suite of melt and fluid inclusions from Ascension Island granite xenoliths. In their rocks, the first exsolved brine (at 0% crystallization) had 41 wt% Cl, corresponding to 67 wt% NaCl if calculated on a NaCl-equivalent basis. After 50% subsequent crystallization the brine was calculated to contain 28 wt% Cl, and after 99.99% crystallization 14 wt% Cl, highlighting that the exsolved single-phase fluid during the major degassing stage is always a brine. At 50 MPa and 100 MPa, the model melt of Cline and Bodnar (1991) attains saturation at about 2.7 and 4 wt% water, corresponding to 8 and 39% crystallization, respectively (Fig. 5). Because fluid-melt partition coefficients for chlorine are much smaller, the initial bulk fluid has a salinity of only 1 wt% NaCl at MPa, and 7 wt% NaCl at 100 MPa. At both conditions, the fluid immediately separates into low-density vapour and brine. At 50 MPa, the vapour has 0.2 wt% NaCl, the brine 70 wt% NaCl, and the initial vapour/brine ratio by mass is about 75 (Fig. 4). At 100 MPa, the vapour has 2.2 wt% NaCl, the brine 50 wt% NaCl, and the initial vapour/brine ratio by mass is about 9. Thus, aqueous fluid is incapable of removing much chlorine

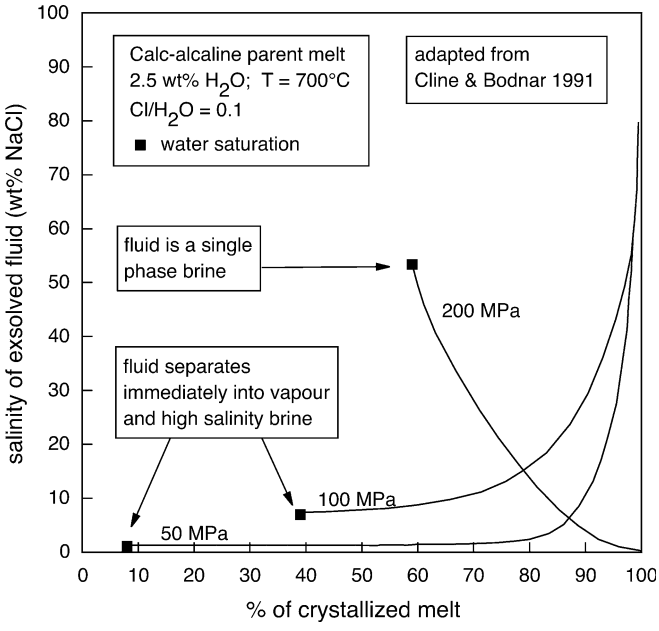

Fig. 5 Salinity of exsolved fluid vs. fraction of crystallized calc-alkaline parent melt with 2.5 wt% water and an initial Cl/H_2O ratio of 0.1 at 700°C and various pressures. *Squares* indicate salinity of first fluids when saturation of the melt is attained. At 50 and 100 MPa, first fluids separate into high-salinity brine and low-density vapour. At 200 MPa, the first fluid is single-phase brine. *Solid lines* denote salinities of evolving fluids as melt crystallization proceeds. At 50 and 100 MPa, increasing bulk salinities indicate increasing brine-vapour ratios with ongoing crystallization. Diagram is adapted from Cline and Bodnar (1991), which in turn is based on experimental data of Shinohara et al. (1984, 1989)

from the melt at the initial degassing stage. As crystallization proceeds, more chlorine is partitioned into the exsolving fluids. Because vapour and brine coexist along a tie-line in P–T–X space and are isobarically and isothermally univariant, increasing bulk chlorine concentrations result simply in increasing brine/vapour ratios at their respective compositions (Figs. 4 and 5; see also Shinohara et al. 1989; Williams et al. 1995; Webster 1997; Webster et al. 1999). Brine/vapour ratios dramatically shift towards the end of the process so that at 100 MPa after about 95% crystallization vapour is absent and a single brine with 50 wt% NaCl is expelled.

It can be shown that this exemplary degassing model is generally valid. It holds, in principle, for different magma compositions, water-chlorine ratios of the melts, varying P–T conditions and also if additional volatiles such as fluorine are present (cf. above). Given the fact that calc-alkaline melts contain chlorine in concentrations between 0.1 and 0.45 wt% and alkaline melts even more, exsolution of pure water is impossible. While the composition of emanating fluids into contact-metamorphic rocks may vary during the complex degassing history of an intrusion, it is certainly true that they are *not* pure water but brines of variable salinity at almost all stages. Even vapour is considerably saline if exsolved at low pressure near the respective critical points of the water–salt system. If vapour with very low salinity is formed far from the critical point it has very low density, and only small amounts of water are transported far into calcareous country rocks. On the other hand, one can reasonably assume that at low pressure two immiscible fluids, brine and vapour, are already present at the inlet of host rocks, i.e. before any decarbonation occurred. If so, they would move along separate pathways (Yardley and Bottrell 1988). Initial two-fluid flow influx may well account for the irregular stable isotope and mineral reaction patterns in near-contact rocks observed in many low-pressure aureoles (cf. above). To our knowledge, this effect has not been considered so far.

Apatite is a common accessory mineral in contact metamorphic marbles and metaargillites and the use of its halogen concentrations to make estimates of aqueous fluid compositions in igneous and metamorphic environments is well established (for reviews see Piccoli and Candela 2002; Spear and Pyle 2002). It has been argued that peak metamorphic fluids at the wollastonite isograd of Mt. Morrison Pendant contact metamorphic rocks (Ferry et al. 2001) and in the periclase zone of the Monzoni aureole (Ferry et al. 2002) probably did not contain significant dissolved salts because most apatites contain no detectable chlorine, with some exceptions of apatites with 2–4 mol% chlorapatite component at Monzoni. This argument is, however, inconclusive as long as fluorine and hydroxyl concentrations are not determined. In fluid-dominated systems, the halogen concentrations in apatite are controlled by the activity ratios a_{HCl}/a_{H_2O} and a_{HF}/a_{H_2O} in the fluid, as well as temperature and pressure. Fluorine is partitioned into apatite much more strongly than is chlorine (e.g. Spear and Pyle 2002, their Fig. 28). Consequently, the vast majority of apatites from felsic to intermediate igneous rocks, metamorphic rocks, and particularly hydrothermal systems are fluorapatites with very low chlorine contents, and many of them are virtually chlorine-free (Piccoli and Candela 2002, their Fig. 5; Spear and Pyle 2002, their Fig. 1). High availability of fluorine prevents incorporation of chlorine into apatite. This has been demonstrated for apatite-fluid exchange in contact-metamorphic aquifers from the Bufa del Diente aureole, NE-Mexico. At about 600°C and 100 MPa, brines of magmatic origin having salinities of 67 to 73 wt% $(NaCl + KCl)_{eq}$ and a_{HF}/a_{H_2O} of about 0.01 crystallized fluorapatite with $FAp_{0.96}CAp_{0.01}HAp_{0.03}$, i.e. with chlorine concentrations in the range of 0.1 wt% (Heinrich 1994). Thus, very low Cl contents of apatite do not necessarily imply coexistence of low salinity fluids. Moreover, estimations of fluid salinities via halogen concentrations in OH-bearing minerals are problematic when fluids are two-phase at low pressure and high temperature. Hydrolysis occurs within the solvus of the simple H_2O–NaCl system due to the reaction $H_2O + NaCl \Leftrightarrow HCl + NaOH$. HCl is strongly fractionated into vapour so that at 50 MPa and 600°C, the quench pH of vapour is about four, and that of brine about ten (Shmulovich et al. 1995; see also Bischoff et al. 1996; Shmulovich et al. 2002). If boiling occurs at given P–T conditions, the brine becomes even more basic. Its

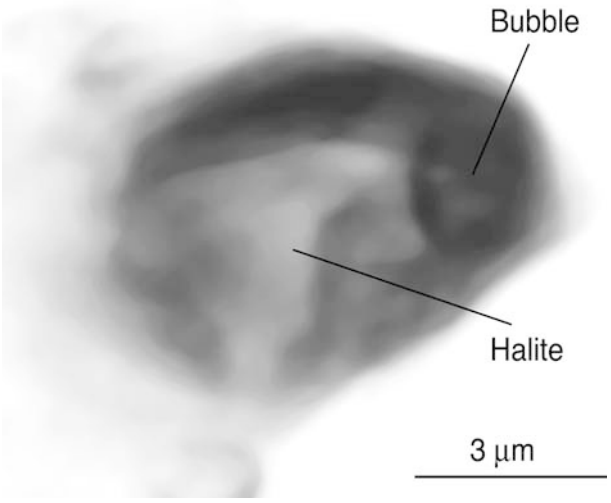

Fig. 6 Small fluid inclusion (6 µm in diameter) in vesuvianite host from the Eastern part of the Monzoni aureole, containing halite (bright crystal with an edge length of about 3 µm). The sample is a calc-silicate fels from the contact north of the "Lago delle Selle" (Masch and Huckenholz 1993), with melilite + grandite + wollastonite + vesuvianite as major phases

salinity continuously increases but its HCl fugacity decreases. As a result, chemically active acidic vapours and alkaline brines are produced, as the two fluids are separated and no longer able to interact with each other. It is clear that in such systems the relation between salinity and HCl fugacity is not straightforward and inferring salinities from halogen concentrations in minerals might be misleading, aside from the fluorine argument. Finally, there is direct evidence that high salinity brines infiltrated the inner Monzoni contact-metamorphic aureole. Very small fluid inclusions (up to 5 µm in diameter) with a large halite daughter crystal were trapped in vesuvianite hosts from melitite-bearing calcsilicates (Fig. 6). Volume estimations indicate salinities of about 50 wt% NaCl.

Effects of fluid separation on mineral reactions

A simple example of reaction-induced fluid segregation at isothermal and isobaric conditions

In a series of seminal papers, Trommsdorff and Skippen (1986, 1987) and Skippen and Trommsdorff (1986) explored the principles of fluid evolution paths generated by decarbonation/dehydration reactions that occur within the solvus of the H_2O–CO_2–salt system. Most relevant is decarbonation, and we illustrate that by examining the reaction diopside + calcite ⇔ akermanite + CO_2 triggered through brine infiltration into calcsilicate-bearing marble at the Bufa del Diente aureole, NE Mexico. A small-scale infiltration profile is selected because it reflects the simplest case of fluid-triggered reaction progress at isothermal and isobaric conditions.

Fig. 7a–f Evolution of the reaction diopside + calcite ⇔ akermanite + CO_2 along a 10 cm wide profile from metaargillite layer into overlying marble from the Bufa del Diente aureole, quarry south-east of the intrusion. **a** Metargillite and wollastonite bands in marbles. Note large vesuvianite idioblasts within the metargillite band. Sample points in marble refer to thin section denotations *b–f*. **b** Fluid inclusions in calcite crystals at point *b* showing high salinity brines with NaCl and KCl daughter crystals coexisting with H_2O–CO_2-rich inclusions. **c** Interstitial melilite within calcite matrix at point *c*. There are no diopside remnants here. **d** Diopside (*yellow-brownish*) at point *d*, almost completely replaced by melilite. **e** Thin rims of melilite around diopside at point *e*. **f** Intact diopsides at point *f*. Here and further into overlying marble, melilite is absent as are fluid inclusions. For compositional details see Heinrich and Gottschalk (1994)

The characteristics of the BD aureole has been described by Heinrich (1993), Heinrich and Gottschalk (1994, 1995) and we focus on a location at the Cañada Piletas quarry south-east of the intrusion where the contact between alkali syenite and marble is perfectly exposed. Estimated P–T conditions close to the contact were 680 ± 20°C and about 120 MPa (Heinrich and Gottschalk 1994). There is mineralogical and isotopic evidence that thick-bedded impure marbles were impervious to magmatic fluids. Aside from a narrow 7–12 m wide zone directly adjacent to the contact, the fluid evolution in marble was internally buffered. Because infiltration was absent, typical "wollastonite-zone" assemblages consisting of calcite + diopside + wollastonite + alkalifeldspar + titanite developed that coexisted with a single H_2O–CO_2–fluid. In contrast, subhorizontal calcareous argillite bands acted as contact-metamorphic aquifers. They were completely decarbonated up to at least 180 m from the contact, resulting in melilite + wollastonite + phlogopite + vesuvianite + perovskite—bearing assemblages. Fluid inclusions trapped in melilite and vesuviante are very rare and too small (≤ 2 µm) for reliable measurements.

The evolution of the reaction diopside + calcite ⇔ akermanite + CO_2 from the metaargillite-marble boundary into overlying marble is traced at sample point BB6, about 30 m from the contact (Fig. 7). The profile illustrates progressive replacement of previously formed prograde clinopyroxene (Fig. 7f) by melilite along a distance of 10 cm towards the aquifer (Fig. 7c–e). Large fluid inclusions, both high salinity brines with $(NaCl + KCl)_{eq} \approx 65$ wt%, $Na/Na + K \approx 0.5$ as well as CO_2-bearing vapour-rich inclusions, are abundant in cores of calcite (Fig. 7b). Further into the marble, clinopyroxene is intact and fluid inclusions are absent. Clinopyroxene is nearly pure diopside with very low Na and small Al_2O_3 contents, melilite compositions range from $Ak_{50}Sm_{50}$ to $Ak_{70}Sm_{30}$ and are free of gehlenite component (Heinrich and Gottschalk 1994). The reaction textures along with the presence of inclusions with conjugate fluids, and sodamelilite component in melilite indicate that the reaction was controlled by brine infiltration from aquifer into marble, fluid immiscibility and subsequent fluid segregation at

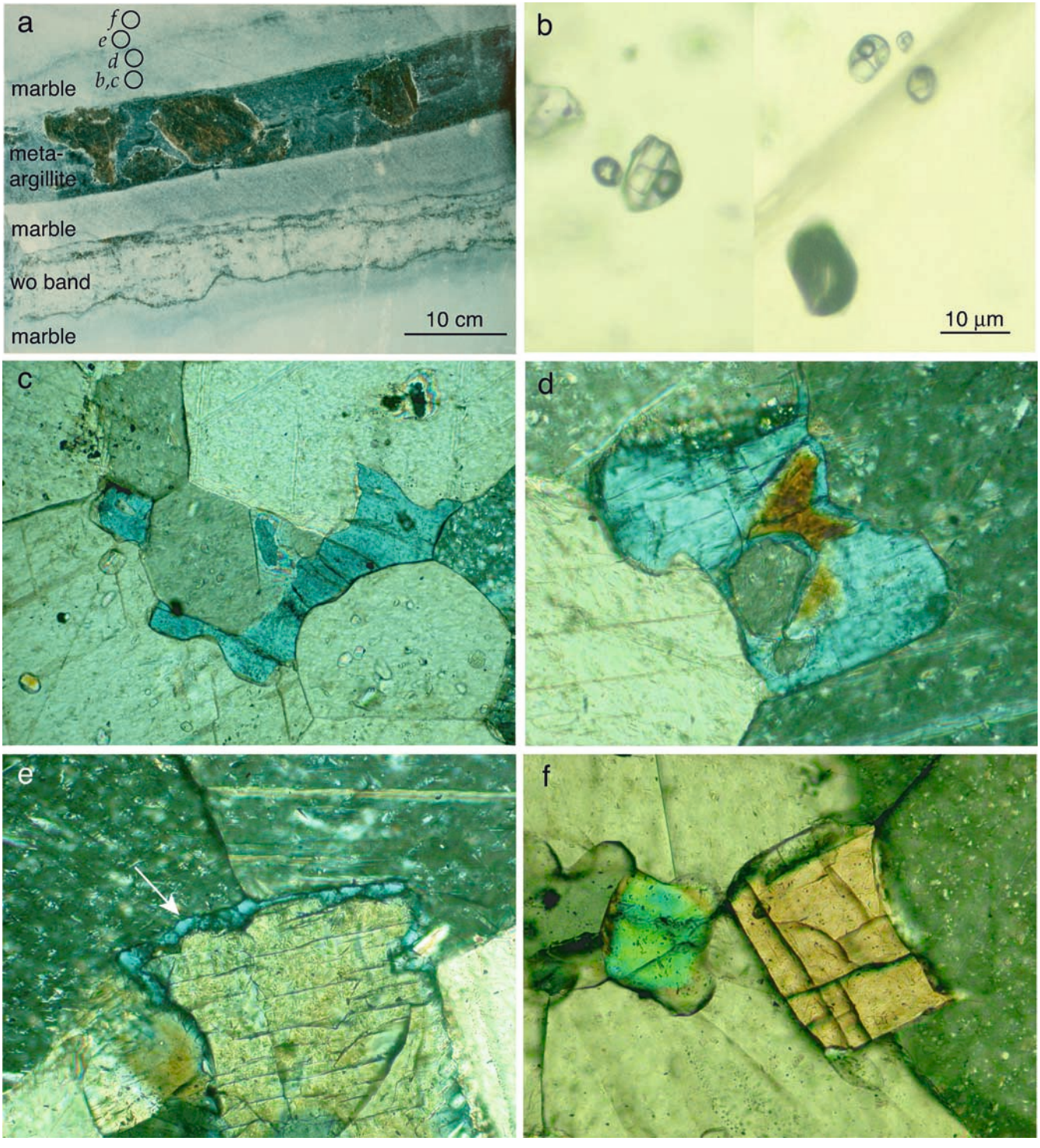

constant P–T-conditions, and that infiltration occurred not earlier than at peak temperatures. The process is recorded along a scale of 10 cm.

The progress of the reaction depends on the position of the fluid solvus boundary relative to the reaction curve, which is very sensitive to small variations in pressure and temperature (Fig. 8). Three isothermal isobaric sections are calculated for 660, 680, and 700°C at 120 MPa, $a_{Di} = 1$, $a_{Ak} = 0.5$, and the simplified H_2O–CO_2–NaCl fluid system. The KCl component of the fluid is neglected implying that the fluid solvus of the natural system is probably somewhat more expanded than shown in Fig. 8. Nevertheless, the crucial point of fluid immiscibility is nicely illustrated. If CO_2-free brine infiltrated the marble at 660°C, the reaction would have occurred within the one-fluid field, independent of salinity (Fig. 8a). The reaction progress would have been very small, particularly at initial brine salinities of

>10 mol% NaCl, and the reaction would have stopped when the brine had dissolved about 1 mol% of the generated CO_2. Only minute amounts of melilite would have been produced. If the infiltrating brine were already CO_2-saturated at about 3–5 mol% CO_2 (corresponding to 10–60 mol% NaCl) no reaction would have taken place. In this case, the conventionally used fluid–rock buffer system would sufficiently describe the infiltration-driven decarbonation process. At 680°C, there is a very small field where the reaction curve intersects the solvus. Fluid immiscibility may occur for infiltrating brines having NaCl concentrations between 4 and 14 mol% (Fig. 8b). The assemblage Cc + Di + Mel (Fig. 7e) cannot coexist with brine having salinities of >14 mol%, however. Given maximum salinities of about 65 wt% detected in fluid inclusions, it is most likely that the reaction occurred at 700°C, provided that pressure is correctly estimated at 120 MPa (Fig. 8c). At these conditions, any NaCl–H_2O fluid at the inlet is just single-phase, irrespective of salinity (Fig. 4). As the reaction started, minute amounts of produced CO_2 drove the fluid into the solvus. Water-rich CO_2-bearing fluid exsolved and the salinity of the brine increased with proceeding reaction along the profile (arrows in Fig. 8c). The reaction terminated when the brine arrived at 30 mol% NaCl corresponding to 58 wt% NaCl, broadly in line with the observed salinity of fluid inclusions. Having attained their respective equilibrium compositions (circles in Fig. 8c) both fluids could move without inducing further reaction, as long as no pressure or temperature gradients existed. The brine did not reach salt saturation because the gap between the reaction curve and the solvus boundary increases towards the NaCl apex. This revises earlier interpretations of Heinrich and Gottschalk (1994) who, due to the lack of an appropriate EOS for immiscible fluids, speculated that the brine reached salt saturation and that, with ongoing reaction, all of the H_2O were transferred to the CO_2-bearing fluid phase. A striking point is that large fluid inclusions are only abundant along the 10 cm wide reaction profile. Obviously, significant entrapment occurred only where the two conjugate fluids were actually produced by boiling.

This simple small-scale example illustrates a common process in the inner portions of contact metamorphic aureoles: decarbonation induced by brine infiltration, fluid immiscibility and fluid segregation. Sharp mineral zone boundaries occurring on a centimetre-scale and often interpreted as isograds probably result from this process. Progress of calc-silicate reactions driven by reactive fluids and resulting fluid flows are delicately dependent on each particular reaction in P–T space relative to the solvus of the H_2O–CO_2–salt system, which in turn drastically expands with increasing temperature and decreasing pressure. It is clear that examination of this process on an aureole-scale, where large temperature gradients exist and pressure gradients are temporarily built up, becomes a very difficult task.

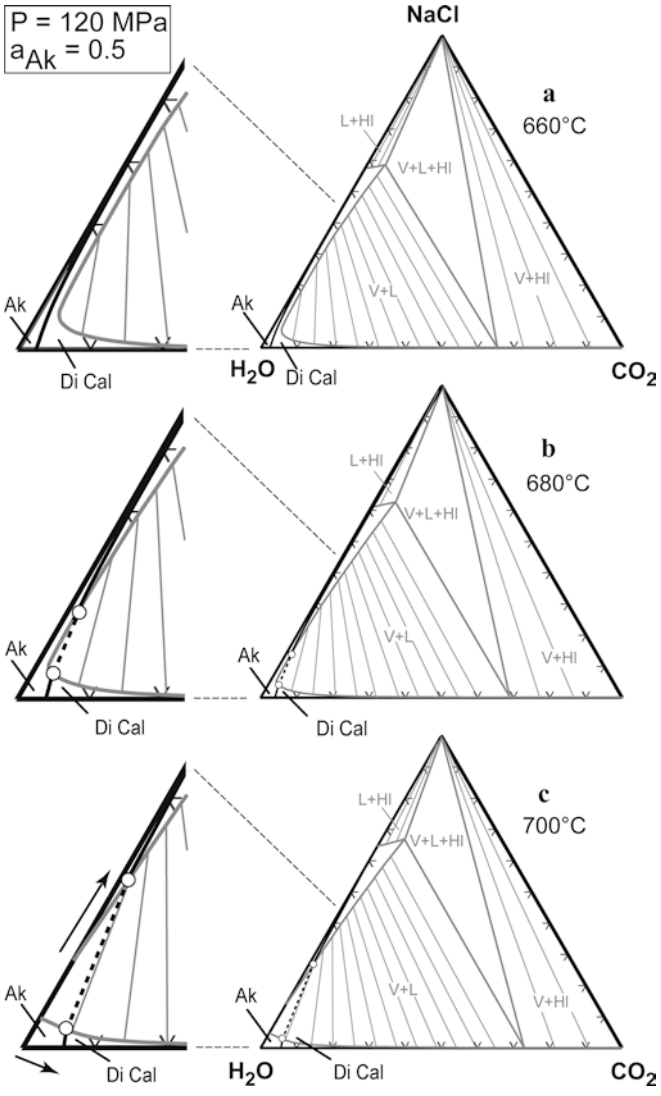

Fig. 8a–c Isobaric isothermal sections of the system H_2O–CO_2–NaCl at 120 MPa and 660°C (**a**), 680°C (**b**) and 700°C (**c**) with the position of the reaction Cc + Di = Ak + CO_2 calculated for $a_{Ak} = 0.5$ (Gottschalk and Heinrich 1994). Components are given in mol%. *Dashed line* connects two coexisting fluids stable with Cc + Di + Ak. At 700°C, *circles* indicate the intersections of the reaction curve with the two-fluid solvus. The brine has about 58 wt% NaCl, the vapour 6 wt% NaCl at $X_{CO_2} = 0.06$. *Arrows* indicate the compositional evolution of the two fluids along which melilite formation may have occurred (see text)

Fluid immiscibility across an aureole-scale temperature gradient and the significance of wollastonite isograds

In their overviews of prograde metamorphic fluid flow through carbonate rocks in selected aureoles, Baumgartner and Valley (2001) and Ferry et al. (2002) altogether cited five locations where pressure during infiltration-driven metamorphism was in the range of 50 MPa. Phase relations from Fig. 3 show that at 450°C and above, traces of salt in the fluid are sufficient for all reactions to proceed within the two fluid solvus. Coming up to higher pressures, the solvus shrinks. Specific

decarbonation reactions may then proceed in the inner aureole within and in outer portions outside the solvus. This is illustrated using the simple model reaction calcite + quartz ⇔ wollastonite + CO_2 at 150 MPa (Fig. 9). Phase relations show that at 500 and 550°C the reaction occurs always with a one-phase water-rich fluid, irrespective of salinity. The reaction curve cuts the solvus at 560°C at moderate salinities. Towards higher temperatures, the reaction proceeds within the solvus. Above 640°C it occurs again with a single phase fluid which now is CO_2-rich and NaCl-free, and in presence of halite instead of brine.

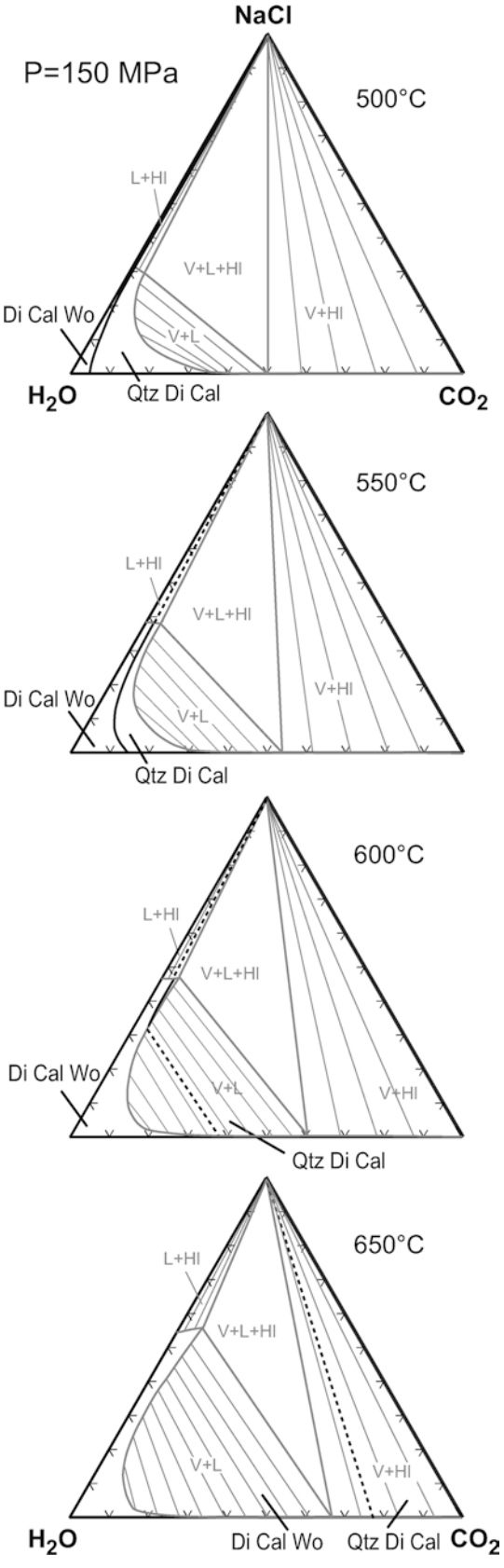

Many field studies have shown that the spatial distribution of wollastonite produced by Cal + Qtz ⇔ Wo + CO_2 records the geometry of infiltration-driven fluid flow in rocks with quartz and calcite as main constituents (e.g. Heinrich 1993; Ferry et al. 2001; Nabelek 2002). Characteristically, sharp reaction fronts developed, separating the upstream part, where decarbonation has gone to completion, from the downstream part, where no reaction occurred. These reaction fronts are conventionally recognized as infiltration isograds (cf. above). If one follows our arguments that magmatic fluid is rather brine than pure water some important implications result. One is that there is a distinct temperature window during which reaction induced fluid immiscibility may occur, comprising about 560–640°C for Cal + Qtz ⇔ Wo + CO_2 at 150 MPa (Fig. 9). During brine infiltration the prograde reaction initially proceeds in the presence of one fluid and changes to two-fluid behaviour above 560°C. As fluid flow advances further into the aureole, reaction induced fluid immiscibility and segregation may take place down to a point where the peak temperature is about 560°C. Beyond that, down-temperature fluid flow triggering the reaction would again change from immiscibility to miscibility. Similarly, infiltration of late retrograde fluids would shift the system back to fluid miscibility along the whole aureole during cooling.

Infiltration-driven wollastonite isograds have been mapped in calcite-bearing contact-metamorphic sandstones from the Mt. Morrison pendant, California (Ferry et al. 2001) and in calc-silicate layers and interfaces between calc-silicate and carbonate layers from the Notch Peak aureole, Utah (e.g. Nabelek and Labotka 1993; Nabelek 2002; Cui et al. 2003). Intrusions are granitoids and pressure was estimated close to 150 MPa in both cases. Peak temperature at the wollastonite isograd was 560°C at Mt. Morrison based on mineral equilibria (Ferry et al. 2001), and somewhat below 550°C at Notch Peak based on heat flow esti-

Fig. 9 Isobaric isothermal sections of the system H_2O–CO_2–NaCl at 150 MPa and 500, 550, 600, and 650°C for composition A denoting the position of the reaction Cal + Qz ⇔ Wo + CO_2. Components are given in mol%. At 500 and 550°C, Cal + Qz + Wo always coexist with one fluid, and at very high salinities, together with single fluid + halite. At 600°C, Cal + Qz + Wo may coexist with brine (about 60 wt% NaCl) plus H_2O + CO_2-fluid ($XCO_2 = 0.38$), or only with brine having more than 60 wt% NaCl. At 650°C, Cal + Qz + Wo coexist with an H_2O–CO_2-fluid of $X_{CO_2} = 0.78$ plus halite, and brine is not stable with this assemblage

mates (Nabelek and Labotka 1993; Nabelek 2002). Infiltration of brine was not considered, but was most likely following our arguments from above. If so, it is striking that the position of the wollastonite isograd in both aureoles coincides with that temperature where reaction-induced fluid segregation caused by brine influx would halt. This is also seen at the Bufa del Diente aureole, NE-Mexico, where brine infiltration and fluid immiscibility has been demonstrated. In carbonate-hosted metachert aquifers the wollastonite isograd appears at 470 ± 10°C (Heinrich 1993; Heinrich et al. 1995). Pressure was estimated at 70 ± 20 MPa based on compositions and densities of fluid inclusions (Heinrich and Gottschalk 1995), and the Cal + Qtz $\Leftrightarrow$ Wo + CO_2 reaction curve coincides with the solvus boundary of the H_2O–CO_2–NaCl system at these conditions. We would argue that this coincidence is not accidental. This would mean that the position of infiltration-driven wollastonite isograds, i.e. the outer bounds of the main down-temperature flow, were *determined* by the P–T–X conditions up to which fluid immiscibility occurred. In fact, wollastonite isograds have been interpreted as representing the boundaries between a high aqueous fluid-flux region on its higher-grade side and up-temperature, low fluid flux on its lower-grade side (e.g. Nabelek 2002; Cui et al. 2003) with different geometries of the flow system observed in the inner and outer portions of an aureole (Ferry et al. 2001; Cui et al. 2003). Fluid immiscibility in the inner portions would easily explain the different flow regimes. Conventional interpretation says that preferential flow of (homogeneous) aqueous fluids within wollastonite zones is promoted by volume loss of the solids and increased pore pressure due to CO_2 production (cf. above). Permeability is transiently increased (e.g. Buick and Cartwright 2002; see also Milsch et al. 2003) and buoyancy forces are believed to drive fluid flow upward and down-temperature near intrusion wall-rock contacts (e.g. Nabelek 2002). An important point is that with advancing down-temperature reactive flow the produced CO_2 must be removed from the reaction sites in order to maintain the reaction. This process, however, is difficult to interpret if infiltration of pure water and a homogeneous H_2O–CO_2 fluid is assumed. Several possibilities have been suggested, such as diffusional transport in a stagnant fluid away from the reaction front (Labotka et al. 1988), diffusion of water against the back flow created by decarbonation and CO_2 production at the front (Balashov and Yardley 1998), strong local fluid expulsion at the front followed by dilution of CO_2-rich fluids by further infiltration of magmatic water, or by dilution with CO_2-poor sedimentary fluid, which may be present beyond the reaction front in the cooler portions of an aureole (Cui et al. 2003). In contrast, reaction-induced fluid immiscibility and segregation, ''boiling'', provides a simple and effective mechanism for removal of exsolved low-density, salt-poor H_2O–CO_2 vapour away from the front. Yardley and Bottrell (1988) pointed out that, where two immiscible fluids coexist, whichever is being produced by reaction will tend to move out of the rock and leave the other behind, and that solid–fluid reactions are strongly enhanced in the presence of immiscible and segregating fluids. That the main fluid flow was confined to portions of the three aureoles where reaction-induced immiscibility may have occurred, may result from this behaviour. One may thus speculate that the entire patterns of magmatic fluid flow into aureoles were ultimately controlled by reaction-induced fluid immiscibility and fluid segregation. This is apart from pre-metamorphic structural controls such as bedding, lithologic contacts, and faults.

A remark on the interpretation of oxygen isotope patterns

Models based on treatment of continuum mechanics in porous media that combine homogeneous fluid flow with mineral reactions and oxygen isotopic exchange have attempted to show that the spatial disposal of such fronts as well as the geometry of the isotopic front itself can be used to determine, or to speculate on, important parameters of fluid–rock interaction during contact metamorphism (for a summary see Baumgartner and Valley 2001). These include: composition and sources of fluids, migration pathways and direction of fluid flow, time-integrated fluxes, fluid transport mechanisms in terms of advection/diffusion/dispersion, validity and degree of local mineralogical and isotopic equilibrium, isotope exchange kinetics, and time-spans of fluid–rock interaction. If one accepts our arguments that during infiltration-controlled reaction progress an additional fluid phase appears, the scenario becomes much more complex than previously thought. A two-fluid flow regime is established in the inner part of the aureole. Fluids could move separately, nevertheless, their footprints recorded in the rocks at different times may overlap in space. With regard to oxygen isotopes, the emergence of a second fluid would affect their distribution behaviour. Little is known about mineral–fluid fractionation factors for high salinity fluids, and nothing about fractionations between brine and salt-poor, low-density H_2O–CO_2 vapour. There are some hints from experiments performed in the pure H_2O–NaCl system up to 600°C and 50 MPa (Shmulovich et al. 1999). $^{18}O/^{16}O_{(L-V)}$ equilibrium fractionation is a linear function of salinity and is about 2‰ at all temperatures near salt saturation. Simple boiling in the H_2O–NaCl system produces isotopically light vapour and heavier brine. Simple decarbonation such as Cal + Qtz $\Leftrightarrow$ Wo + CO_2 produces CO_2 enriched in ^{18}O. The system becomes substantially complex and one may expect that salt-poor vapours with varying H_2O/CO_2 ratios in equilibrium with brine + solids would develop a wide range in $^{18}O/^{16}O$ isotope ratios as brine changes salinity and oxygen isotopic composition along its pathway.

Conclusions

Having presented the arguments for magmatic fluids being saline and for infiltration-driven decarbonation reactions occurring within the H_2O–CO_2–NaCl fluid solvus at contact-metamorphic conditions we are forced towards an uncomfortable conclusion: Time-integrated fluid fluxes estimated by combining fluid advection/dispersion models with the spatial arrangement of mineral reactions and isotopic resetting that have been presented by many authors for numerous aureoles (e.g. Ferry and Gerdes 1998; Baumgartner and Valley 2001; Ferry et al. 2002; and references therein) may be spurious because fluid immiscibility is disregarded. In calcareous rocks, fluid segregation inevitably takes place at low pressures of contact-metamorphism within the inner, hotter parts of aureoles. Immiscible fluids will move separately, thus imposing different stable isotope patterns on minerals along their pathways. The process is, among many others, mainly controlled by the salinity of the infiltrating brine, which may drastically vary during the devolatilization history of the magma, and by the relative locations of mineral reactions and the H_2O–CO_2–salt solvus in P–T–X space, which are highly sensitive to very small pressure and temperature variations. If so, the history of two-phase fluid flow might be completely different in each particular aureole. Global reviews on reactive fluid flow coupled with progress of calc-silicate reactions and stable isotope shifts in contact aureoles are certainly valuable. However, a closer look at mineral assemblages, stable isotope profiles and fluid inclusions, on both a large and small scale, would help in identifying complex fluid flux behaviour and provide insight into what really happened with these fascinating rocks.

Acknowledgements We thank Kirill Shmulovich for stimulating discussions. Reiner Schulz and Heike Steigert made most of the drawings. Soraya Heuss-Assbichler kindly provided thin sections from the Monzoni aureole. The paper benefited from many critical comments by Rainer Abart.

References

Balashov VN, Yardley BWD (1998) Modeling metamorphic fluid flow with reaction-compaction-permeability feedbacks. Am J Sci 298:441–470

Baumgartner L, Valley JW (2001) Stable isotope transport and contact-metamorphic fluid flow. In: Valley JW, Cole DR (eds) Stable isotope geochemistry (Reviews in mineralogy and geochemistry, vol 43) Mineral Soc Am, Washington, pp 415–467

Bischoff JL, Rosenbauer RJ, Fournier RO (1996) The generation of HCl in the system $CaCl_2$–H_2O: vapour–liquid relations from 380 to 500°C. Geochim Cosmochim Acta 60:7–16

Bodnar RJ, Burnham CW, Sterner SM (1985) Synthetic fluid inclusions in natural quartz: III. Determination of phase equilibrium properties in the system NaCl–H_2O to 1000°C and 1500 bars. Geochim Cosmochim Acta 49:1861–1873

Bowers TS, Helgeson HC (1983a) Calculation of the thermodynamic and geochemical consequences of nonideal mixing in the system H_2O–CO_2–NaCl on phase relations in geological systems: equation of state for H_2O–CO_2–NaCl fluids at high pressures and temperatures. Geochim Cosmochim Acta 47:1247–1275

Bowers TS, Helgeson HC (1983b) Calculation of the thermodynamic and geochemical consequences of nonideal mixing in the system H_2O–CO_2–NaCl on phase realtions in geological systems: metamorphic equilibria at high pressures and temperatures. Am Mineral 68:1059–1075

Bowman JR, Willett SD, Cook SJ (1994) Oxygen isotopic transport and exchange during fluid flow: one-dimensional models and applications. Am J Sci 294:1–55

Buick IS, Cartwright I (2002) Fractured-controlled fluid flow and metasomatism in the contact aureole of the Marulan Batholith (New South Wales, Australia). Contrib Mineral Petrol 143:733–749

Cartwright I (1997) Permeability geration and resetting of tracers during metamorphic fluid flow: implications for advection-dispersion models. Contrib Mineral Petrol 129:198–208

Cartwright I, Buick IS (1996) Determining the direction of contact metamorphic fluid flow: an assessment of mineralogical and stable isotope criteria. J Metamorph Geol 14:289–305

Cline JS, Bodnar JB (1991) Can economic porphyry copper mineralization be generated by a typical calc-alkaline melt? J Geophys Res 96-B5:8113–8126

Cook SJ, Bowman JR, Forster CB (1997) Contact metamorphism surrounding the Alta Stock: finite element model simulation of heat- and $^{18}O/^{16}O$ mass-transport during prograde metamorphism. Am J Sci 297:1–55

Cui X, Nabelek PI, Liu M (2003) Reactive flow of mixed CO_2–H_2O fluid and progress of calc-silicate reactions in contact metamorphic aureoles: insight from two-dimensional numerical modelling. J Metamorph Geol 21:663–684

Dipple GM, Ferry JM (1996) The effect of thermal history on the development of mineal assemblages during infiltration driven contact metamorphism. Contrib Mineral Petrol 124:334–345

Duan Z, Møller N, Weare JH (1995) Equation of state for the NaCl–H_2O–CO_2 system: prediction of phase equilibria and volumetric properties. Geochim Cosmochim Acta 59:2869–2882

Fernandez-Caliani JC, Casquet C, Galán E (1996) Complex multiphase fluid inclusions in wollastonite from the Mérida contact-metamorphic deposit, Spain: evidence for rock/HCl-rich fluid interaction. Eur J Mineral 8:1015–1026

Ferry JM (1995) Fluid flow during contact metamorphism of ophiocarbonate rocks in the Bergell aureole, Val Malenco, Italian Alps. J Petrol 36:1039–1053

Ferry JM (1996) Prograde and retrograde fluid flow during contact metamorphism of siliceous carbonate rocks from the Ballachulish aureole, Scotland. Contrib Mineral Petrol 124:235–254

Ferry JM, Rumble D III (1997) Formation and destruction of periclase by fluid flow in two contact aureoles. Contrib Mineral Petrol 128:313–334

Ferry JM, Gerdes ML (1998) Chemically reactive fluid flow during metamorphism. Annu Rev Earth Planet Sci 26:255–287

Ferry JM, Sorensen SS, Rumble D III (1998) Structually controlled fluid flow during contact metamorphism in the Ritter range pendant, California, USA. Contrib Mineral Petrol 130:358–378

Ferry JM, Wing BA, Rumble D III (2001) Formation of wollastonite by chemically reactive flow during contact metamorphism, Mt. Morrison Pendant, Sierra Nevada, California, USA. J Petrol 42:1705–1728

Ferry JM, Wing BA, Penniston-Dorland SC, Rumble D III (2002) The direction of fluid flow during contact metamorphism of siliceous carbonate rocks: new data for the Monzoni and Predazzo aureoles, northern Italy, and a global review. Contrib Mineral Petrol 142:679–699

Gehrig M (1980) Phasengleichgewichte und PVT-Daten ternärer Mischungen aus Wasser, Kohlendioxid und Natriumchlorid bis 3 Kbar und 550°C. Hochschulverlag Freiburg, Germany

Gerdes ML, Baumgartner LP, Person M, Rumble D III (1995) One and two dimensional models of fluid flow and stable isotope exchange at an outcrop in the Adamello contact aureole, Southern Alps, Italy. Am Mineral 80:1004–1019

Gottschalk M (1997) Internally consistent thermodynamic data set for rock forming minerals in the system SiO_2–TiO_2–Al_2O_3–Fe_2O_3–CaO–MgO–FeO–K_2O–Na_2O–H_2O–CO_2: an alternative approach. Eur J Mineral 9:175–223

Gottschalk M, Metz P (1992) The system calcite-dolomite: a model to calculate the Gibbs free energy of mixing on the basis of existing experimental data. N Jb Min Abh 164:29–55

Heinrich W (1993) Fluid infiltration through metachert layers at the contact aureole of the Bufa del Diente intrusion, northeast Mexico: implications for wollastonite formation and fluid immiscibility. Am Mineral 78:804–818

Heinrich W (1994) Potassium-fluor-richterite in metacherts from the Bufa del Diente contact-metamorphic aureole, NE–México. Mineral Petrol 50:259–270

Heinrich W, Gottschalk M (1994) Fluid flow patterns and infiltration isograds in melilite marbles from the Bufa del Diente contact metamorphic aureole, north-east Mexico. J Metamorph Geol 12:345–359

Heinrich W, Gottschalk M (1995) Metamorphic reactions between fluid inclusions and mineral hosts I: progress of the reaction calcite + quartz $\Leftrightarrow$ wollastonite + CO_2 in natural wollastonite-hosted fluid inclusions. Contrib Mineral Petrol 122:51–61

Holness MB (1997) Fluid flow paths and mechanisms of fluid infiltration in carbonates during contact metamorphism: the Beinn an Dubhaich aureole, Skye. J Metamorph Geol 15:59–70

Holness MB, Fallick AE (1997) Palaeohydrology of the calcsilsicate aureole of the Beinn an Dubhaich granite, Skye, Scotland: a stable isotope study. J Metamorph Geol 15:71–83

Jamtveit B, Bucher-Nurminen K, Stijfhoorn DE (1992a) Contact metamorphism of layered shale-carbonate sequences in the Oslo Rift: I. Buffering, infiltration, and the mechanisms of mass transport. J Petrol 33:377–422

Jamtveit B, Grorud HF, Bucher-Nurminen K (1992b) Contact metamorphism of layered carbonate-shale sequences in the Oslo Rift. II. Migration of isotopic and reaction fronts around cooling plutons. Earth Planet Sci Lett 114:131–148

Jamtveit B, Andersen T (1993) Contact metamorphism of layered shale-carbonate sequences in the Oslo Rift: III. Nature of skarn-forming fluids. Econ Geol 88:1830–1849

Labotka TC, Nabelek PI, Papike JJ (1988) Fluid infiltration through the Big Horse Limestone in the Notch Peak contact-metamorphic aureole, Utah. Am Mineral 73:1302–1324

Lowenstern JB (1994) Chlorine, fluid immiscibility, and degassing in peralkaline magmas from Pantelleria, Italy. Am Mineral 79:353–369

Lowenstern JB (1995) Applications of silicate melt inclusions to the study of magmatic volatiles. In: Thompson JFH (ed) Magmas, fluids, and ore deposits. Mineral Assoc Can Short Course 23:71–99

Masch L, Huckenholz G (1993) Der Intrusivkomplex von Monzoni und seine thermometamorphe Aureole. Beih Eur J Mineral 5:81–135

Mercolli I (1982) Le inclusione fluide nei noduli di quarzo dei marmi dolomitici della regione de Campolungo (Ticino). Schweiz Mineral Petrogr Mitt 62:245–312

Milsch H, Heinrich W, Dresen G (2003) Reaction-induced fluid flow in synthetic quartz-bearing marbles. Contrib Mineral Petrol 146:286–296

Nabelek PI, Labotka TC, Ross-Labotka C (1992) Stable isotope evidence for the role of diffusion, infiltration, and local structure on contact metamorphism of calc-silicate rocks at Notch Peak, Utah. J Petrol 33:557–583

Nabelek PI, Labotka TC (1993) Implications of geochemical fronts in the Notch Peak contact metamorphic aureole, Utah, USA. Earth Planet Sci Lett 119:539–559

Nabelek PI (2002) Calc-silicate reactions and bedding controlled isotopic exchange in the Notch Peak aureole, Utah: implications for differential fluid fluxes with metamorphic grade. J Metamorphic Geol 20:429–440

Piccoli PM, Candela PA (2002) Apatite in igneous systems. In: Kohn MJ, Rakovan J, Hughes JM (eds) Phosphates (Reviews in mineralogy and geochemistry, vol 48). Mineral Soc Am, Washington, pp 255–292

Povoden E, Horacek M, Abart R (2002) Contact metamorphism of siliceous dolomite and impure limestones from the Werfen Formation in the eastern Monzoni contact aureole. Mineral Petrol 76:99–120

Shinohara H (1994) Exsolution of immiscible vapour and liquid phases from a crystallizing silicate melt: implications for chlorine and metal transport. Geochim Cosmochim Acta 58:5215–5222

Shinohara H, Iiyama JT, Matsuo S (1984) Geochemistry-behaviour of chlorine in the system granitic magma-hydrothermal solution (in French). CR Acad Sci Paris Ser II 298:741–743

Shinohara H, Iiyama JT, Matsuo S (1989) Partition of chlorine compounds between silicate melts and hydrothermal solutions. I. Partition of NaCl–KCl. Geochim Cosmochim Acta 53:2617–2630

Shmulovich KI, Tkachenko SI, Plyasunova NV (1995) Phase equilibria in fluid systems at high pressures and temperatures. In: Shmulovich KI, Yardley BWD, Gonchar GG (eds) Fluids in the crust. Chapman and Hall, London, pp 193–214

Shmulovich KI, Landwehr D, Simon K, Heinrich W (1999) Stable isotope fractionation between liquid and vapour in water–salt systems. Chem Geol 157:343–354

Shmulovich K, Heinrich W, Möller P, Dulski P (2002) Experimental determination of REE fractionation between liquid and vapour in the systems NaCl–H_2O and $CaCl_2$–H_2O up to 450°C. Contrib Mineral Petrol 144:257–273

Sisson VB, Crawford ML, Thompson PH (1981) CO_2-brine immiscibility at high temperatures: evidence from calcareous metasedimentary rocks. Contrib Mineral Petrol 78:371–378

Skippen G, Trommsdorff V (1986) The influence of NaCl and KCl on phase relations in metamorphosed carbonate rocks. Am J Sci 286:81–104

Spear FS, Pyle JM (2002) Apatite, monazite, and xenotime in metamorphic rocks. In: Kohn MJ, Rakovan J, Hughes JM (eds) Phosphates (Reviews in mineralogy and geochemistry, vol 48). Mineral Soc Am, Washington, pp 293–335

Trommsdorff V, Skippen G, Ulmer P (1985) Halite and sylvite as solid inclusions in high-grade metamorphic rocks. Contrib Mineral Petrol 89:24–29

Trommsdoff V, Skippen G (1986) Vapour loss (“boiling”) as a mechanism for fluid evolution in metamorphic rocks. Contrib Mineral Petrol 94:317–322

Trommsdorff V, Skippen G (1987) Metasomatism involving fluids in CO_2–H_2O–NaCl. In: Helgeson HC (ed) Chemical transport in metasomatic processes (Proc NATO Advanced Study Inst), Reidel, Dordrecht, pp 133–152

Webster JD (1997) Chloride solubility in felsic melts and the role of chloride in magmatic degassing. J Petrol 38:1793–1807

Webster JD (2002) The exsolution of magmatic brine. Geochim Cosmochim Acta 66:(spec suppl 15A):A826 (abstr)

Webster JD, Kinzler RJ, Mathez EA (1999) Chloride and water solubility in basalt and andesite melts and implications for magmatic degassing. Geochim Cosmochim Acta 63:729–738

Webster JD, Rebbert CR (2001) The geochemical signature of fluid-saturated magma determined from silicate melt inclusions in Ascension Island granite xenoliths. Geochim Cosmochim Acta 65:123–136

Webster JD, DeVivo B (2002) Experimental and modelled solubilities in aluminosilicate melts, consequences of magma evolution, and implications for exsolution of hydrous chloride melt at Mt. Somma–Vesuvius. Am Mineral 87:1046–1061

Williams TJ, Candela PA, Piccoli PM (1995) The partitioning of copper between silicate melts and two-phase aqueous fluids: an experimental investigation at 1 kbar, 800°C and 0.5 kbar, 850°C. Contrib Mineal Petrol 121:388–399

Williams-Jones AE, Ferreira DR (1989) Thermal metamorphism and H_2O–CO_2–NaCl immiscibility at Parapedia, Quebec: evidence from fluid inclusions. Contrib Mineral Petrol 102:247–254

Yardley BWD, Bottrell SH (1988) Immiscible fluids in metamorphism: implications of two-phase fluid flow for reaction history. Geology 16:199–202